Acta Cryst. (1996). A52, 606–613

MEM Analysis of Electron-Density Distributions for Silicon and Diamond using Short-Wavelength X-rays (W $K\alpha_1$)

K. YAMAMOTO,[a]*† Y. TAKAHASHI,[a] K. OHSHIMA,[a] F. P. OKAMURA[b] AND K. YUKINO[b]

[a]*Institute of Applied Physics, University of Tsukuba, Tsukuba 305, Japan, and* [b]*National Institute for Research in Inorganic Materials, Tsukuba 305, Japan. E-mail: yamamoto@phys.nara-wu.ac.jp*

(Received 12 June 1995; accepted 7 February 1996)

Abstract

Short-wavelength X-rays (W $K\alpha_1$: $\lambda = 0.209$ Å) have been used to collect higher-order reflections for studies of the electron-density distributions of silicon and diamond with high resolution. The sp^3 bonding electron-density distributions of these materials are visible in the total electron-density maps synthesized by the maximum-entropy method (MEM) and also in the difference MEM maps synthesized by Fourier summation of $F^{\rm mem}(\mathbf{h}) - F^{\rm core}(\mathbf{h})$, where $F^{\rm mem}(\mathbf{h})$ is the structure factor calculated from the MEM map and $F^{\rm core}(\mathbf{h})$ is the structure factor calculated from Si^{core} and C^{core} models, if very extensive data sets with higher-order reflections are used. These maps are more informative than the conventional difference Fourier map synthesized by Fourier summation of $F^{\rm obs}(\mathbf{h}) - F^{\rm core}(\mathbf{h})$ using the observed structure factor $F^{\rm obs}(\mathbf{h})$ instead of $F^{\rm mem}(\mathbf{h})$. The present maps can be compared with certain band-theory calculations.

1. Introduction

To understand the nature of the chemical bonds in materials precisely, an accurate determination of the electron-density distribution (hereafter EDD) is indispensable. To date, there have been determinations of the many EDDs for silicon, diamond and germanium, both experimentally and theoretically, because of their importance as semiconductors. They also provide typical examples of the covalent bond and are used as standard samples for new experiments and theories. In the last decade, high-accuracy structure factors, within the millielectron range, were measured by some dynamical diffraction techniques such as the *Pendellösung* method. Full or partial data sets of structure factors, which can be used to analyze EDDs, were collected by Aldred & Hart (1973), Teworte & Bonse (1984) and Saka & Kato (1986) and consolidated by Cummings & Hart (1988) for silicon and collected by Takama, Tsuchiya, Kobayashi & Sato (1990) for diamond. Such data sets have been carefully analyzed by many authors. For silicon, Lu & Zunger (1992) compared measured EDDs with *ab initio* theoretical calculations within the local-density formalism. Deutsch (1992) used the multipole expansion for data analysis. Spackman (1986, 1991) derived deformation and valence electron density *via* Fourier summation and used multipole refinement for silicon and diamond. Sakata & Sato (1990) evaluated the precise EDD of silicon by the maximum-entropy method with 30 structure factors measured by Saka & Kato (1986) and concluded that bonding electrons were clearly visible in the MEM map even if the forbidden reflections were excluded. The MEM is very powerful in studying the EDD because of its visual clearness, in particular, in regions of low electron density, and because of the freedom from use of conventional models in the calculation [*e.g.* Sakata & Sato (1990); Yamamoto & Kashida (1991); Sakata, Uno & Mori (1992); Takata, Kubota & Sakata (1993)].

The above studies focused on precision in structure factors of only lower-order reflections. The results deduced from the EDD maps were, therefore, accurate only at low resolution. In order to achieve higher resolution, we have used short-wavelength X-rays (W $K\alpha_1$: $\lambda = 0.209$ Å) and collected many structure factors by single-crystal diffraction up to very high order reflections ($\sin\theta/\lambda < 2.5$ Å^{-1} for silicon; $\sin\theta/\lambda < 3.0$ Å^{-1} for diamond). The high-resolution EDD maps are estimated by analyzing these data sets by the MEM. A difference in the regions of the bonding electrons for silicon and diamond is clearly seen. Bonding electron-density distributions are also estimated by subtraction of core elements within MEM maps. These distributions are compared with the results obtained by certain self-consistent band-structure calculations.

2. Experimental procedures

Data collections were made on the ultra-short-wavelength X-ray generator at the National Institute for Research in Inorganic Materials. Details of the generator have already been described elsewhere (Okamura *et al.*, 1993; Okamura, 1994). The inte-

† Present address: Physics Department, Nara Women's University, Nara 630, Japan.

grated-intensity measurements for silicon and diamond were carried out using W $K\alpha_1$ with an automatic single-crystal four-circle diffractometer. A very high accelerating voltage of 150 kV (×10 mA) was used to obtain an efficient photon flux of W $K\alpha$ radiation, whose exciting voltage is 69.3 kV. The X-ray spectra of this experiment for 80, 100, 120 and 140 kV are shown in Fig. 1. In general, $K\alpha$ lines are separated from white spectra with the use of a monochromator for the conventional case. However, when we use short-wavelength X-rays, the energy resolution of the monochromator becomes poor owing to the small diffraction angle. On the other hand, the energy difference for $K\alpha_1$ and $K\alpha_2$ is large when a target containing a heavy element is used.

In this measurement, we have combined a Ge solid-state detector (Ge-SSD), a pulse-height analyzer (PHA) and a multichannel analyzer (MCA) to measure data for the W $K\alpha_1$ line only without a monochromator. As the energy difference between W $K\alpha_1$ and W $K\alpha_2$ is 1.34 keV and the energy resolution of the Ge-SSD at W $K\alpha$, with a thickness of 15 mm for the Ge crystal, is 0.3–0.4 keV within the time constants of the main amplifier, the W $K\alpha_1$ line is easily selected using the single-channel analyzer by carefully adjusting the window, which has a base line E_B and a width ΔE_W for the PHA (Fig. 2). An Al filter (1–2 cm) is always inserted to avoid counting loss, which reduces the intensity for low-energy reflections generated from white radiation.

For measuring integrated intensities, both angle-dispersive and energy-dispersive methods can be utilized without changing the experimental arrangements. For angle-dispersive X-ray diffraction, the intensity is measured by using the PHA in ω-scan mode. The integrated intensity is then expressed as

$$I_{\rm obs}(\mathbf{h}) \propto |F_{\rm obs}(\mathbf{h})|^2(1+\cos^2 2\theta)/(\sin 2\theta)\lambda^3, \quad (1)$$

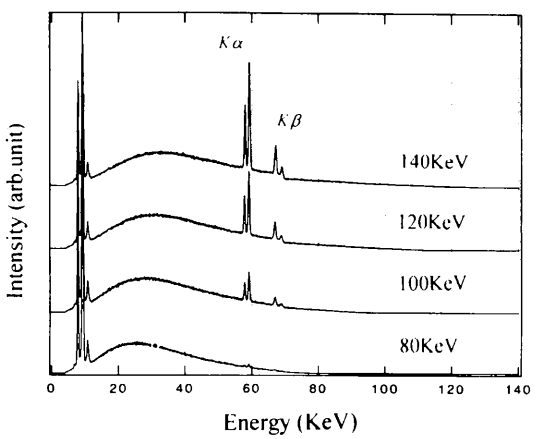

Fig. 1. The observed X-ray spectra of air scattering on the MCA generated at 80, 100, 120 and 140 keV without any correction. The Ge-SSD was fixed at $2\theta = 2°$.

where $F_{\rm obs}(\mathbf{h})$ is an observed structure factor. For energy-dispersive X-ray diffraction, the intensity is measured by using the MCA in fixed-angle mode. The integrated intensity is then expressed as

$$I_{\rm obs}(\mathbf{h}) \propto |F_{\rm obs}(\mathbf{h})|^2(1+\cos^2 2\theta)/(\sin^2\theta)\lambda^4. \quad (2)$$

The intensity becomes weaker at shorter wavelengths. On the other hand, the absorption effect for the specimen becomes weaker at shorter wavelengths. Larger specimens allow measurement of intensities with high efficiency. Silicon and diamond single crystals were, therefore, shaped into spheres of 1.85 and 2.2 mm diameter, respectively. Since the diameter of the collimator is 3.0 mm and the distance between the target and the specimen is 870 mm, the incident beam on the specimen is homogeneous enough to obtain accurate intensities. The setting parameters were carefully determined by the eight setting method (King & Finger, 1979). The main collections of integrated intensities were conducted by the ω-scan mode of an angle-dispersive method. For silicon, reflections in six separate directions $[(+h,+k,+l;\ h \geq k \geq l)$, $(+h,+k,+l;\ l \geq k \geq h)$, $(+h,-k,-l;\ k \geq h \geq l)$, $(-h,+k,+l;\ k \geq l \geq h)$, $(-h,-k,-l;\ l \geq h \geq k)$ and $(-h,+k,-l;\ h \geq l \geq k)]$ of an independent 1/48 volume in reciprocal space were collected up to the $2\theta_{\rm max}$ value of 65°. For diamond, reflections with indices $(+h,+k,\pm l)$ were collected up to the $2\theta_{\rm max}$ value of 80°. The $\sin\theta_{\rm max}/\lambda$ values are 2.57 Å^{-1} for silicon and 3.08 Å^{-1} for diamond. If Ag $K\alpha$ radiation is used, the maximum value for $\sin\theta/\lambda$ is 1.74 Å^{-1}. Therefore, the present measurement is capable of collecting many more integrated intensities compared with conventional measurements. Detailed experimental conditions are summarized in Table 1.

Weak reflections with $|F_{\rm obs}(\mathbf{h})| < 3\sigma(\mathbf{h})$ were excluded from the data set, where $\sigma(\mathbf{h})$ is the standard deviation of the observed structure amplitude due to counting statistics. Forbidden reflections of the

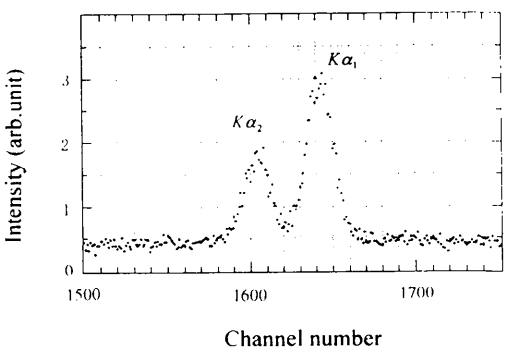

Fig. 2. The observed X-ray spectrum of air scattering on the MCA generated at 140 kV near the $K\alpha$ line. The energies of the $K\alpha_1$ and $K\alpha_2$ lines are 59.318 and 57.982 keV, respectively. The energy difference is 1.337 keV. The energy resolution of the present experiments is 400 eV at 60 keV.

Table 1. *Crystallographic data and experimental conditions*

	Silicon	Diamond
X-ray wavelength (Å)	0.209	0.209
Crystal diameter (mm)	1.85	2.2
Accelerating voltage (kV)	150	150
Applied current (mA)	10	10
Scan mode	ω	ω
Scan speed (° min^{-1})	0.802	0.802
Scan width (°)	0.45	0.55
Collected area in the reciprocal space (sphere)	1/8	1/4
$\sin\theta/\lambda$ range (Å^{-1})	0.0–2.57	0.0–3.08

diamond-type structure ($h+k+l=4n\pm2$) were not collected. The intensities of equivalent reflections were averaged. The values of the internal agreement factor, which is defined by the equation $\sum \big||F_{obs}| - \langle|F_{obs}|\rangle\big| / \sum |F_{obs}|$, were 0.024 for silicon and 0.028 for diamond, respectively. The numbers of independent reflections were 369 for silicon and 209 for diamond, respectively. Corrections for Lorentz and polarization factors were performed. Absorption corrections were made by assuming spherical shapes of the specimens. The linear absorption coefficients are 0.7644 cm^{-1} for silicon and 0.6188 cm^{-1} for diamond, respectively.

3. Data set

In order to analyze the integrated intensities with the use of the MEM, an absolute value and a phase for each structure factor are needed. In addition to the above-mentioned corrections, an absolute scale and an extinction correction must be performed. In particular, in a structure analysis or an analysis to obtain the EDD, the accuracy is seriously affected by the extinction effect. The scale factors and the isotropic extinction parameters, g_{iso}, defined by Zachariasen (1967), and the temperature factors, B, for each of the data sets were refined by the full-matrix least-squares program *RADIEL* (Coppens *et al.*, 1979). In least-squares refinements of each of the data sets, 28 lower-order reflections for silicon and nine lower-order reflections for diamond, which have a large extinction correction [$y(\mathbf{h}) < 0.90$ for silicon and $y(\mathbf{h}) < 0.80$ for diamond], were excluded, where $y(\mathbf{h})$ is defined by $F_{kin}(\mathbf{h}) = F_{obs}(\mathbf{h})/y(\mathbf{h})^{1/2}$. In this equation, $F_{kin}(\mathbf{h})$ is the kinematical structure factor. The number of reflections used in the least-squares refinements are 341 for silicon and 200 for diamond, corresponding to 0.864–2.490 and 0.829–2.993 Å^{-1} in the $\sin\theta/\lambda$ value, respectively. Neutral-atom scattering factors were used. The results of the refinements are summarized in Table 2.

Some accurate and absolute data sets for lower-order reflections of silicon and diamond have already been obtained. We have, therefore, used the lower-order

Table 2. *Values of the temperature factor, B, the isotropic extinction factor, g_{iso}, and reliability factor, R, for silicon and diamond, obtained by the least-squares refinement*

The R factor is expressed as $R = \sum \big||F_{obs}| - |F_{cal}|\big| / \sum |F_{obs}|$.

	Silicon	Diamond
B (Å^2)	0.467 (1)	0.164 (1)
g_{iso} ($\times 10^{-4}$)	11.2 (2)	1.62 (3)
R (%)	2.23	0.96

structure factors that were obtained by Saka & Kato (1986) for 28 reflections of silicon and by Takama, Tsuchiya, Kobayashi & Sato (1990) for 9 reflections of diamond, instead of the excluded ones. The number of reflections used in the MEM calculations are 369 for silicon and 209 for diamond, with $\sin\theta_{max}/\lambda$ values 2.490 and 2.993 Å^{-1}, respectively.

4. MEM calculation

Some kinds of maximum-entropy methods suitable for electron-density refinement have already been described by several authors [*e.g.* Wilkins, Varghese & Lehmann (1983), Wilkins (1983), Bricogne (1984), Livesey & Skilling (1985), Navaza (1986), Sakata & Sato (1990)]. We follow the procedure used by Sakata & Sato (1990) who used the formalism of Collins (1982). Many EDDs have been shown to be synthesized on the basis of this procedure by using a limited number of accurate lower-order reflections, several tens, obtained from powder diffraction pattern analysis [*e.g.* Sakata, Uno & Mori (1992); Takata, Kubota & Sakata (1993)].

In the present study, we collected as many reflections with higher-order indices as possible: the number of reflections was over 300 for silicon and 200 for diamond, in spite of their simple space group. In this case, however, a poor MEM map is usually obtained with many irregular ripples under the ordinary MEM conditions. To solve this problem, we adopt a weighting function, $w(h)$, used by de Vries, Briels & Feil (1994). The electron density at the pixel i, used by Sakata & Sato (1990), can be modified as

$$\rho(\mathbf{r}_i) = \tau(\mathbf{r}_i)\exp\left\{(lF_{000}/N)\sum_{\mathbf{h}}[w(\mathbf{h})/\sigma(\mathbf{h})^2] \times \left[F_{obs}(\mathbf{h}) - F_{cal}(\mathbf{h})\right]\exp(-2\pi i\mathbf{h}\cdot\mathbf{r}_i)\right\}, \quad (3)$$

where

$$F_{cal}(\mathbf{h}) = V\sum_i \tau(\mathbf{r}_i)\exp(2\pi i\mathbf{h}\cdot\mathbf{r}_i). \quad (4)$$

The only difference from Sakata & Sato's original definition is the inclusion of the weighting function $w(\mathbf{h})$. The iterative calculation can start from the uniform electron density and continue until the condi-

tion $C < 1$ is attained, where the constraint equation is expressed as

$$C = (1/N)\sum_{\mathbf{h}}\left[F_{\rm obs}(\mathbf{h}) - F_{\rm cal}(\mathbf{h})\right]^2/\sigma(\mathbf{h})^2. \quad (5)$$

In the MEM calculations, we divided the unit cell into $104 \times 104 \times 104$ pixels. We have tried different weighting schemes and estimated the appropriateness of each case. The following weighting functions are examined:

$$w(\mathbf{h}) = 1, \quad (6)$$

$$w(\mathbf{h}) = F_{\rm obs}(\mathbf{h})^n, \quad n = \tfrac{1}{4}, \tfrac{1}{2}, 1, 2, \ldots, \quad (7)$$

$$w(\mathbf{h}) = [(\sin\theta)/\lambda]^{-n}, \quad n = \tfrac{1}{4}, \tfrac{1}{2}, 1, 2, \ldots, \quad (8)$$

and so forth. It is possible to judge the appropriateness of the choice of $w(\mathbf{h})$ with two factors, *i.e.* an agreement between a histogram of the values

$$\left[|F_{\rm obs}(\mathbf{h})| - |F_{\rm cal}(\mathbf{h})|\right]/\sigma(\mathbf{h}) \quad (9)$$

and a Gaussian distribution (de Vries, Briels & Feil, 1994) and also a homogeneity in the distribution of their values against $\sin\theta/\lambda$.

5. MEM density map

In the present work, it turned out that the best weight function is $w(\mathbf{h}) = [F(\mathbf{h})]^{1/4}$ for the silicon data and $w(\mathbf{h}) = F(\mathbf{h})^4$ for the diamond data. The electron-density maps calculated with the MEM on the $(10\bar{1})$ planes are displayed in Fig. 3(*a*) for silicon and in Fig. 3(*b*) for diamond. The histograms of the values of (9) for each map are shown in Fig. 4(*a*) and in Fig. 4(*b*). The distributions of the value of (9) on $\sin\theta/\lambda$ are shown in Fig. 5(*a*) and Fig. 5(*b*). The desirable EDD maximizes the entropy under the condition $C = 1$ but does not necessarily make the R factor minimum, where $R = \sum\left||F_{\rm obs}(\mathbf{h})| - |F_{\rm cal}(\mathbf{h})|\right|/\sum|F_{\rm obs}(\mathbf{h})|$. For the most reliable map obtained, the C value of any partial regions was always 1 in the data and the values of (9) followed a Gaussian distribution. In the case of diamond, however, it was difficult to make them fit to a Gaussian curve, as seen in Fig. 5(*b*), because of some kind of systematic error in the data. The R factors are 0.0103 for silicon and 0.0104 for diamond.

The bonding electron-density distributions are visible in both the MEM maps. The heights of the electron density at the middle point are $0.568\,\text{e}\,\text{Å}^{-3}$ for silicon and $1.49\,\text{e}\,\text{Å}^{-3}$ for diamond, respectively. This difference reflects the difference of covalency.

In general, it is easy to estimate the structural factors for the forbidden 222 and 442 reflections from the synthesized MEM map but it is difficult to estimate their errors. In the present MEM, the histogram of the values of (9) shows a Gaussian distribution and, furthermore, the distribution of their values against $\sin\theta/\lambda$ is homogeneous. We understand from these facts that the calculated errors $\sigma(F^{\rm cal})$ are rather independent of the observed errors $\sigma(F^{\rm obs})$ of the reflections if the diffraction angles are fairly different. We therefore estimated the standard deviations of structure factors for 222 and 442 reflections to be the averaged value of the standard deviations for five reflections observed around these two reflections.

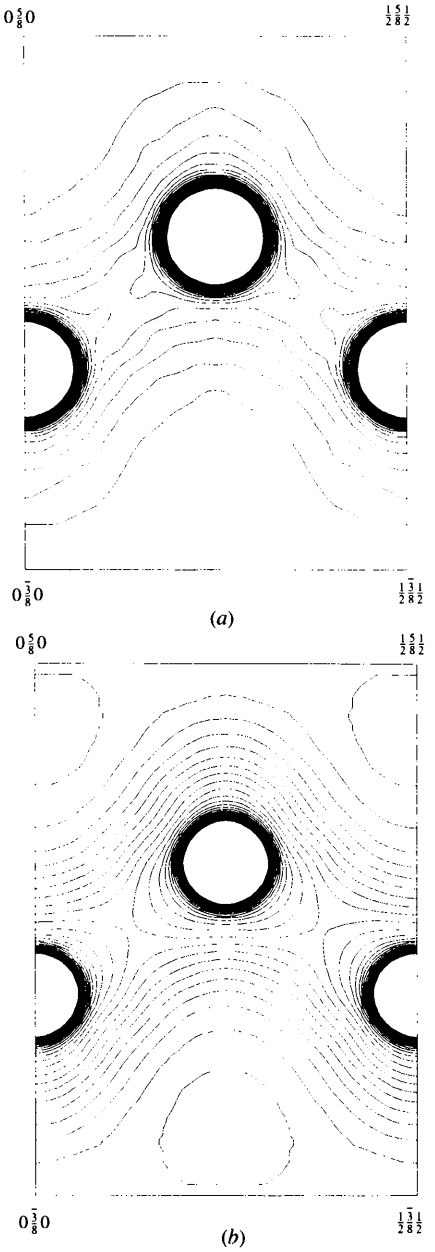

Fig. 3. The electron-density maps calculated with the MEM on the $(10\bar{1})$ plane for (*a*) silicon and (*b*) diamond. The contour lines are drawn from 0.1 to $2.0\,\text{e}\,\text{Å}^{-3}$ with $0.1\,\text{e}\,\text{Å}^{-3}$ intervals for silicon, and from 0.15 to $3.0\,\text{e}\,\text{Å}^{-3}$ with $0.15\,\text{e}\,\text{Å}^{-3}$ intervals for diamond.

6. The covalent bonding electrons

In order to compare the present result with other theoretical and experimental results in detail, we have deduced the distribution of the covalent bonding electrons from the MEM map. To begin with, we defined the covalent-bonding structure factor as

$$F^{\text{bond}}(\mathbf{h}) = F^{\text{mem}}(\mathbf{h}) - F^{\text{core}}(\mathbf{h}), \qquad (10)$$

where $F^{\text{mem}}(\mathbf{h})$ is the structure factor calculated from the MEM map and $F^{\text{core}}(\mathbf{h})$ is the structure factor calculated from the Si^{core} and C^{core} models in which only core electrons are taken into account with the same harmonic temperature factors as those obtained by the refinement in §3. It is worthwhile to point out here that the bonding structure factor defined here is different from the usual $F^{\text{bond}}(\mathbf{h})$, which is defined as $F^{\text{obs}}(\mathbf{h}) - F^{\text{core}}(\mathbf{h})$ instead of $F^{\text{mem}}(\mathbf{h}) - F^{\text{core}}(\mathbf{h})$ of (10). Random errors are usually included in $F^{\text{obs}}(\mathbf{h})$, but are in principle excluded in $F^{\text{mem}}(\mathbf{h})$. $F^{\text{bond}}(\mathbf{h})$ of (10) must be free from such random errors. Atomic scattering factors $f_{\text{Si}}^{\text{core}}$ and $f_{\text{C}}^{\text{core}}$, listed in *International Tables for X-ray Crystallography* (1974) are used. Then the bonding electron density, $\rho_{\text{bond}}(\mathbf{r})$, was synthesized by using the Fourier summation of $F^{\text{bond}}(\mathbf{h})$, where additional forbidden reflections of the diamond-type structure were also included and the number of bonding electrons was fixed to 32 in the unit cell. The Fourier summations were carried out up to the $\sin\theta/\lambda$ value of $2.0\,\text{Å}^{-1}$ for both materials. We refer to the $\rho_{\text{bond}}(\mathbf{r})$ obtained as the difference MEM map, hereafter. The difference MEM maps of the $(10\bar{1})$ plane are shown in Fig. 6(*a*) for silicon and in Fig. 7(*a*) for diamond. It is interesting to compare these maps with the conventional difference Fourier maps of $F^{\text{obs}}(\mathbf{h}) - F^{\text{core}}(\mathbf{h})$ shown in Fig. 6(*b*) and Fig. 7(*b*). It is clear from Fig. 6 and Fig. 7 that the bonding electron density $\rho_{\text{bond}}(\mathbf{r})$ is very smoothly reproduced in the difference MEM maps.

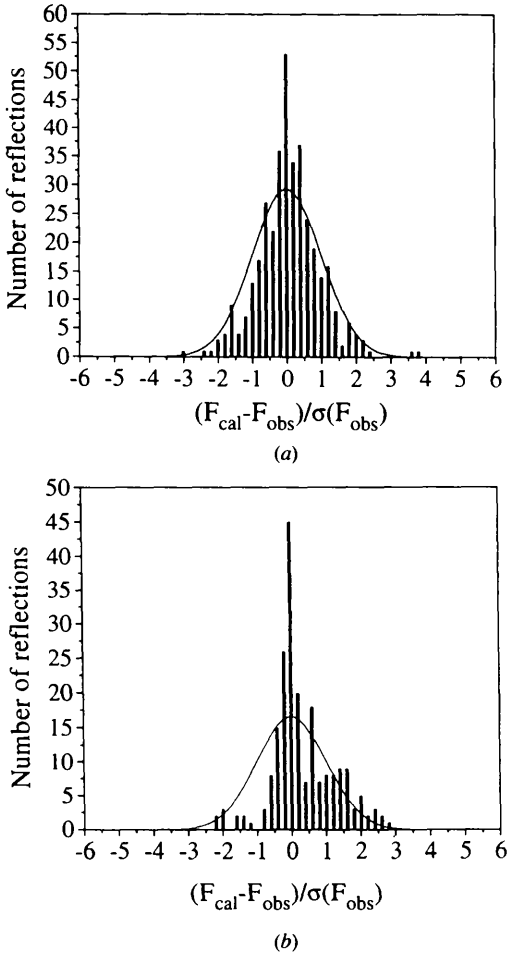

Fig. 4. The histograms of the $[|F_{\text{obs}}(\mathbf{h})| - |F_{\text{cal}}(\mathbf{h})|]/\sigma(\mathbf{h})$ values for (*a*) silicon and (*b*) diamond. The thick solid line is the Gaussian distribution.

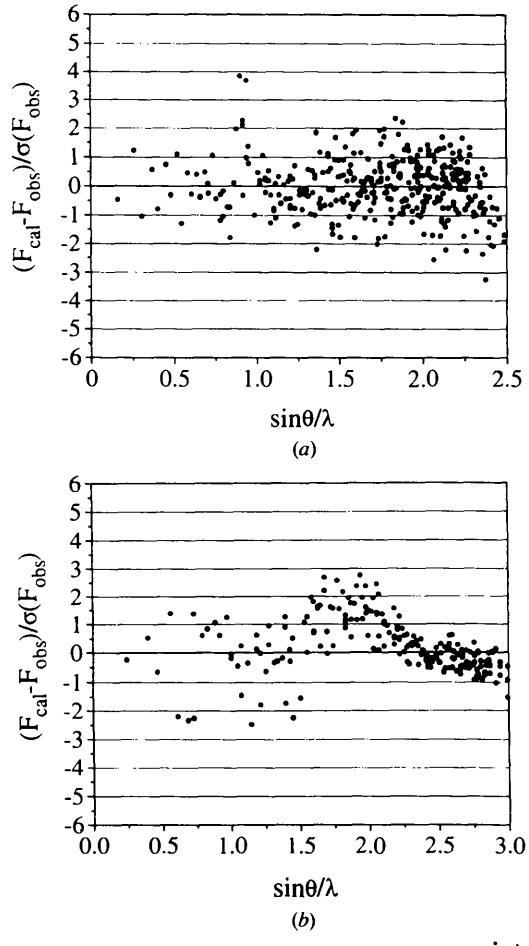

Fig. 5. The $[|F_{\text{obs}}(\mathbf{h})| - |F_{\text{cal}}(\mathbf{h})|]/\sigma(\mathbf{h})$ values *vs* $\sin\theta/\lambda$ (Å^{-1}) for (*a*) silicon and (*b*) diamond.

7. Silicon

The MEM map [Fig. 3(*a*)] shows a broad flat region of electron density between two adjacent atoms. The small projection is detected from the core region possibly due to sp^3 clouds. The difference MEM map [Fig. 6(*a*)] shows it more clearly and displays a weak but distinct twin peak. This map can be compared with theoretical calculations: the calculation based on the *ab initio* pseudopotential method (Yin & Cohen, 1982) and that based on the linear muffin-tin orbital (LMTO) method (Christensen, Satpathy & Pawlowska, 1987) show a single peak between Si atoms; on the other hand, the calculation based on the LMTO method (Weyrich, 1988) and that based on the linear combination of atomic orbitals (LCAO) method (Zandiehnadem & Ching, 1990) show a distinct twin peak, in agreement with the present result. The peaks in Fig. 6(*a*) are located at 0.97 Å from the atomic center. The saddle point on the bonding electron clouds has a value of $0.60\,\mathrm{e\,\AA^{-3}}$.

It is also expected that the intrinsic structure of covalent sp^3 clouds near the Si atom would be visible in the difference MEM map of Fig. 6(*a*) because of high resolution. However, such a structure is not visible owing to the large thermal vibration of silicon.

Sakata & Sato (1990) have shown that the structure factors of the 222 and 442 forbidden reflections calculated from the MEM map are in good agreement with those measured by different experiments. We have also carried out this approach from each map. The structure factors for the 222 and 442 reflections were calculated to be 1.571 (5) and −0.047 (9), respectively (see §5 for the estimation of the standard deviation), in agreement with Sakata & Sato (1990) with small differences that are slightly larger than the estimated standard deviation. These differences are considered to correspond to inhomogeneity in the distribution of their values against $\sin\theta/\lambda$.

8. Diamond

The MEM map (Fig. 3*b*) shows a strong connection of the electron density between two adjacent C atoms. The wide projection is detected from the core regions owing to sp^3 clouds compared with silicon. The difference MEM map (Fig. 7*a*) shows a strong and distinct twin peak located at 0.32 Å from the atomic center. The saddle point on the bonding electron clouds has a value of $1.96\,\mathrm{e\,\AA^{-3}}$, which is three times larger than that of silicon. In Figs. 3(*b*) and 6(*b*), the shapes of the electron density and a residual electron density near the atomic position are almost spherical. This means that the C atom vibrates harmonically. These maps can also be compared with theoretical calculations of EDDs by Chelikowsky & Louie (1984) with the linear combination of atomic like orbitals (LCAO) method and by Christensen, Satpathy & Pawlowska (1987) with the LMTO method. A similar complete twin peak to that in Fig. 7(*a*) is reproduced by these theoretical calculations.

In the difference MEM map of Fig. 7(*a*), the intrinsic structure of covalent sp^3 clouds is revealed near the C atom, clearly indicating an effect of high resolution. We can assume that the thermal vibration is not as large as that of the Si atom.

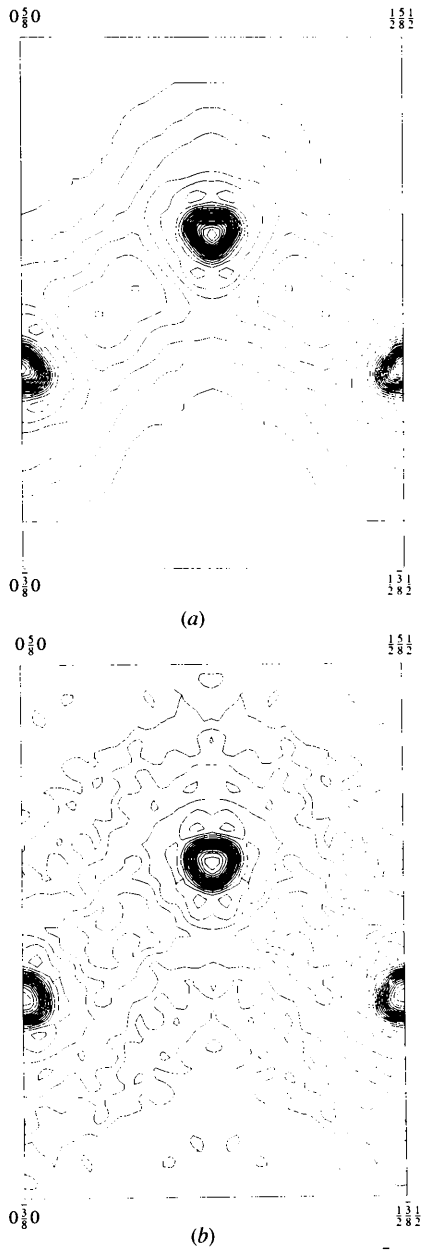

Fig. 6. The bonding electron-density maps on the $(10\bar{1})$ plane for silicon: (*a*) the difference MEM map and (*b*) the conventional difference Fourier map. The contour lines are drawn from 0.1 to $2.0\,\mathrm{e\,\AA^{-3}}$ with $0.1\,\mathrm{e\,\AA^{-3}}$ intervals.

The structure factors for the 222 and 442 reflections were calculated to be 0.98(6) and −0.04(3), respectively.

9. Discussion

In the EDDs of silicon and diamond, sp^3 electron distributions are elongated along the bond direction and these shapes are wholly similar. The obvious difference is seen in the bonding electron-density maps: diamond has a characteristic peak close to the atom position, while silicon has a large island consisting of a weak twin peak. These express a difference of the intrinsic distribution between the $2s2p^3$ wave function of diamond and the $3s3p^3$ wave function of silicon.

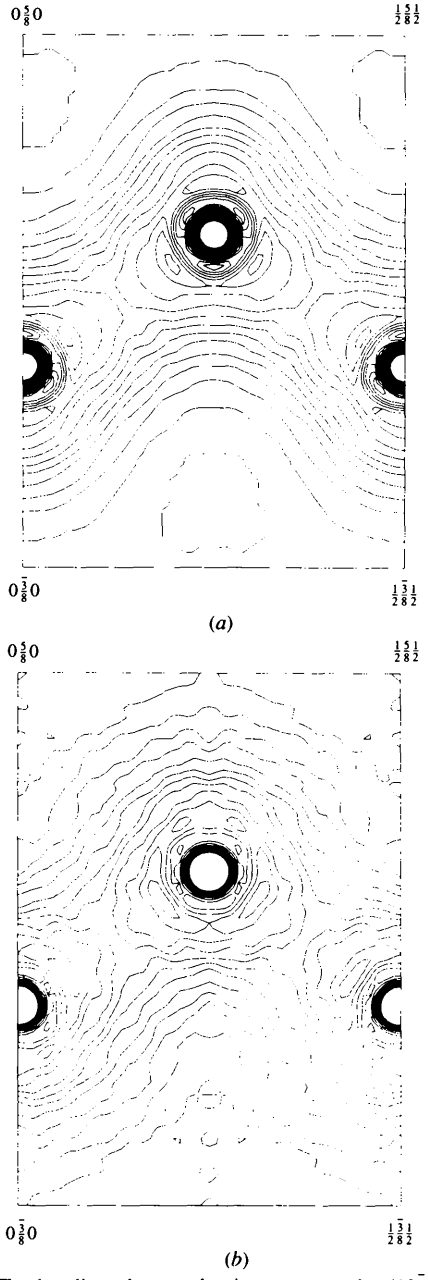

Fig. 7. The bonding electron-density maps on the $(10\bar{1})$ plane for diamond: (*a*) the difference MEM map and (*b*) the conventional difference Fourier map. The contour lines are drawn from 0.15 to 3.0 e Å^{-3} with 0.15 e Å^{-3} intervals.

It is obvious from the present study that when more reflections are used in MEM calculations a better MEM map is obtained with higher resolution. In discussing EDD, the difference MEM map of $F^{\rm mem}(\mathbf{h}) - F^{\rm core}(\mathbf{h})$ is more informative than the conventional difference Fourier map of $F^{\rm obs}(\mathbf{h}) - F^{\rm core}(\mathbf{h})$ because the conventional difference Fourier map is affected by random errors so that non-physical ripples usually appear in the map. The intrinsic structure of sp^3 clouds near the C-atom core would not be revealed if the MEM map was reproduced without including higher-order reflections with high accuracy. Thus, we conclude that the inclusion of higher-order reflections is very important in MEM calculations.

In order to discuss the intrinsic structure of covalent sp^3 clouds near the Si atom, however, we need to reduce the large thermal vibration by taking measurements at low temperature.

We can apply this technique to obtain the accurate electron-density distributions of any materials. It would be interesting to study, in particular, the heavier elements such as the lanthanide compounds.

The authors would like to thank Dr Y. Sato of NIRIM for kindly supplying diamond single crystals, and Toshiba Ceramics Co. for kindly supplying silicon single crystals.

References

Aldred, P. J. E. & Hart, M. (1973). *Proc. R. Soc. London Ser. A*, **332**, 223–238, 239–254.

Bricogne, G. (1984). *Acta Cryst.* A**40**, 410–445.

Chelikowsky, J. R. & Louie, S. G. (1984). *Phys. Rev. B*, **29**, 3470–3481.

Christensen, N. E., Satpathy, S. & Pawlowska, Z. (1987). *Phys. Rev. B*, **36**, 1032–1050.

Collins, D. M. (1982). *Nature (London)*, **298**, 49–51.

Coppens, P., Guru Row, T. N., Leung, P., Stevens, E. D., Becker, P. J. & Yang, Y. W. (1979). *Acta Cryst.* A**35**, 63–72.

Cummings, S. & Hart, M. (1988). *Aust. J. Phys.* **41**, 423–431.

Deutsch, M. (1992). *Phys. Rev. B*, **45**, 646–657.

International Tables for X-ray Crystallography (1974). Vol. IV. Birmingham: Kynoch Press. (Present distributor Kluwer Academic Publishers, Dordrecht.)

King, H. E. Jr & Finger, L. W. (1979). *J. Appl. Cryst.* **12**, 374–378.

Livesey, A. L. & Skilling, J. (1985). *Acta Cryst.* A**41**, 113–122.

Lu, Z. W. & Zunger, A. (1992). *Acta Cryst.* A**48**, 545–554.

Navaza, J. (1986). *Acta Cryst.* A**42**, 212–223.
Okamura, F. P. (1994). *Rigaku J.* **11**, 15–21.
Okamura, F. P., Yukino, K., Yamamoto, K., Hoshikawa, K., Hori, T., Yoshimachi, S., Yokoyama, R., Kawasaki, H., Tsukamoto, K. & Izawa, H. (1993). *Acta Cryst.* A**49**, C375.
Saka, T. & Kato, N. (1986). *Acta Cryst.* A**42**, 469–478.
Sakata, M. & Sato, M. (1990). *Acta Cryst.* A**46**, 263–270.
Sakata, M., Uno, T. & Mori, R. (1992). *Acta Cryst.* B**48**, 591–598.
Spackman, M. A. (1986). *Acta Cryst.* A**42**, 271–281.
Spackman, M. A. (1991). *Acta Cryst.* A**47**, 420–427.
Takama, T., Tsuchiya, K., Kobayashi, K. & Sato, S. (1990). *Acta Cryst.* A**46**, 514–517.
Takata, M., Kubota, Y. & Sakata, M. (1993). *Z. Naturforsch. Teil A*, **48**, 75–80.
Teworte, R. & Bonse, U. (1984). *Phys Rev. B*, **29**, 2102–2108.
Vries, R. Y. de, Briels, W. J. & Feil, D. (1994). *Acta Cryst.* A**50**, 383–391.
Weyrich, K. H. (1988). *Phys. Rev. B*, **37**, 10269–10282.
Wilkins, S. W. (1983). *Acta Cryst.* A**39**, 892–896.
Wilkins, S. W., Varghese, J. H. & Lehmann, M. S. (1983). *Acta Cryst.* A**39**, 47–60.
Yamamoto, K. & Kashida, S. (1991). *Solid State Ionics*, **48**, 241–248.
Yin, M. T. & Cohen, M. L. (1982). *Phys. Rev. B*, **26**, 5668–5687.
Zachariasen, W. H. (1967). *Acta Cryst.* **23**, 558–564.
Zandiehnadem, F. & Ching, W. Y. (1990). *Phys. Rev. B*, **41**, 12162–12179.